

Three particles in a finite volume: The breakdown of spherical symmetry

Simon Kreuzer* and Harald W. Griebhammer†

*Institute for Nuclear Studies, Department of Physics,
The George Washington University, Washington DC 20052, USA*

(Dated: July 25, 2018)

Abstract

Lattice simulations of light nuclei necessarily take place in finite volumes, thus affecting their infrared properties. These effects can be addressed in a model-independent manner using Effective Field Theories. We study the model case of three identical bosons (mass m) with resonant two-body interactions in a cubic box with periodic boundary conditions, which can also be generalized to the three-nucleon system in a straightforward manner. Our results allow for the removal of finite volume effects from lattice results as well as the determination of infinite volume scattering parameters from the volume dependence of the spectrum. We study the volume dependence of several states below the break-up threshold, spanning one order of magnitude in the binding energy in the infinite volume, for box side lengths L between the two-body scattering length a and $L = 0.25a$. For example, a state with a three-body energy of $-3/(ma^2)$ in the infinite volume has been shifted to $-10/(ma^2)$ at $L = a$. Special emphasis is put on the consequences of the breakdown of spherical symmetry and several ways to perturbatively treat the ensuing partial wave admixtures. We find their contributions to be on the sub-percent level compared to the strong volume dependence of the S-wave component. For shallow bound states, we find a transition to boson-diboson scattering behavior when decreasing the size of the finite volume.

arXiv:1205.0277v1 [nucl-th] 1 May 2012

* E-Mail: skreuzer@gwu.edu (corresponding author)

† E-Mail: hgrie@gwu.edu

I. INTRODUCTION

Quantum chromodynamics (QCD) is the theory underlying strong interactions. However, ab initio calculations of hadronic and nuclear properties remain one of the largest theoretical challenges of the Standard Model. Lattice simulations provide a numerical approach, but do at present not usually operate at the physical point (for reviews on the lattice simulations of light nuclei see, e.g., [1, 2]). In a complementary approach, Effective Field Theories (EFT) describe the effective degrees of nuclear physics, namely nucleons and pions, and allow for accurate calculations of low-energy observables with a direct link to QCD through the symmetries of the theory, see e.g. [3–8].

In lattice simulations, the QCD path integral is evaluated in a discretized Euclidean space-time using Monte-Carlo simulations. This approach requires a large numerical effort, which in turn strongly constrains the parameters of the simulation. In particular, the considered system is necessarily placed in a finite volume. Present day calculations use cubic boxes with periodic boundary conditions and relatively small side lengths of a few fm. Momentum quantization due to the boundary conditions causes a shift of the finite-volume spectrum relative to the infinite-volume energies [9]. A model-independent determination of this shift is necessary in order to extract physical observables from lattice results. Calculations at large volumes are possible, but rendered inefficient by the enormous numerical effort necessary. Therefore, the use of well-known physics to perform the extrapolation is warranted.

The volume dependence of the spectrum also provides access to scattering parameters. Most prominently, Lüscher showed that infinite volume scattering phase shifts as well as resonance properties are encoded in the finite-volume spectrum of two-particle states [10, 11].

The correlation function for the three-nucleon system in the triton channel has been calculated in Lattice QCD recently [12], but because of the relatively large uncertainties no triton properties could be extracted. With quantitative lattice data on light nuclei and their scattering properties within reach, Lüscher’s results need to be extended to the three-body sector in order to understand the finite volume effects in these results.

The desired incorporation of well-known physics, combined with the demand of model independence and the ability to achieve a given level of accuracy, are preconditions well met by the EFT approach. In the nuclear sector, the pionless EFT, which is valid for processes with typical momenta below the pion mass, has been successfully used to describe the properties of light nuclei (see, e.g., [3, 4, 6] for reviews). To leading order, the three-body sector is described by the nucleon-nucleon scattering lengths in the 1S_0 and 3S_1 channels and a Wigner SU(4) symmetric three-body force [13–15].

The pionless EFT in the nucleonic sector can be seen as part of a larger family of EFTs for systems with resonant two-body interactions. They are characterized by the appearance of a two-body scattering length a that is unnaturally large compared to the range of interaction. Such systems display interesting universal properties. If a is positive, two particles of mass m form a shallow two-body bound state with binding energy $1/(ma^2)$, independent of the detailed mechanism generating the large scattering length. For example, ^4He atoms have the unnaturally large scattering length $189 a_0$, where a_0 is the Bohr radius. Using the aforementioned relation to extract a from the energy of the helium dimer, on the other hand, yields a scattering length of $182 a_0$, deviating by only 3.7%. In the pionless EFT, the shallow two-body bound state is identified as the deuteron.

In the three-body system, the universal properties include the Efimov effect [15]. If at least two of the three particles have a scattering length $|a|$ that is large compared to the

range of their interaction, a sequence of three-body bound states exists. In the limit of diverging scattering length, there are infinitely many geometrically spaced bound states with an accumulation point at threshold. This spectrum is the signature of the Efimov effect, namely a discrete scaling symmetry whose consequences can be calculated in an EFT for short-range interactions. Here, it appears because the renormalization group flow of the three-body coupling is a limit cycle (see, e.g., [16, 17] for a review). This is the case for the Wigner $SU(4)$ symmetric three-body force in pionless EFT [13], but also for the three-body force needed to renormalize the simpler EFT of three identical bosons [18]. In this work, we will therefore study systems of three identical bosons inside a cubic box with periodic boundary conditions using the EFT framework. Transferring the methods developed in this publication to the pionless EFT will give an understanding of the finite volume corrections in lattice calculations of the three-nucleon system.

In this paper, we study the volume dependence of three-boson states below the three-body break-up threshold inside a cubic box with periodic boundary conditions. One of the authors performed similar studies before [19–22]. We developed the new framework presented in this paper for several reasons. First, the new approach provides access to the energy region above the boson-diboson break-up threshold. Second, it does not rely on the use of basis functions but remains in close contact with the discrete space of allowed momenta. It further allows for a faster numerical implementation when higher partial waves are taken into account. Thus, for the first time, we are able to study the size of these higher partial wave contributions in a systematic manner as well as how they can be included perturbatively.

The application of EFT to finite volumes, especially for three-particle systems, has sparked interest in recent years. The volume dependence for three spin-1/2 fermions with perturbative interactions in a box has been studied previously [23]. Epelbaum and collaborators have calculated the energy of the triton in a finite volume by implementing a discretized version of chiral EFT on a lattice [24]. Also, the triton has been considered in pionless EFT in a nuclear lattice formalism but the volume dependence was not investigated [25]. Other volume shapes have also been studied, most prominently the harmonic oscillator [26, 27], which allows to compute finite volume effects inside atomic traps.

This paper is organized as follows. In the next Section, we derive the basic equations and sketch the ideas of our numerical implementation. We furthermore present two different approaches to include higher partial wave corrections perturbatively. In Section III, we provide a detailed discussion of our numerical results, including a study on the perturbative nature of higher partial waves. Section IV summarizes our findings and provides an outlook for future work.

II. FRAMEWORK

In the following, we derive a set of coupled equations governing the partial waves of the amplitude and explain how to prepare these equations for a numerical implementation. In the last part of this section, we show two ways to take higher partial waves into account perturbatively.

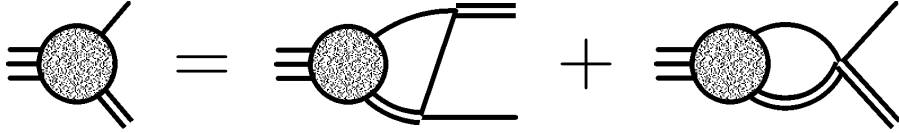


FIG. 1. Integral equation for the boson-diboson amplitude, represented by the shaded circle. The single line denotes the single boson, while the double line denotes the diboson field.

A. Sum equation for the amplitude

The Lagrangian for three identical bosons interacting via short-range forces can be written as (see, e.g., [17, 18])

$$\mathcal{L} = \psi^\dagger \left(i\partial_t + \frac{1}{2}\nabla^2 \right) \psi + \frac{g_2}{4} d^\dagger d - \frac{g_2}{4} (d^\dagger \psi^2 + \text{H.c.}) - \frac{g_3}{36} d^\dagger d \psi^\dagger \psi + \dots, \quad (1)$$

where the dots indicate higher order terms of the effective theory. The Lagrangian is formulated in terms of the boson field ψ and a non-dynamical auxiliary field d with the quantum numbers of two bosons. Units have been chosen such that $\hbar = m = 1$, where m is the mass of a single boson.

The system of three bosons is assumed to be contained in a cubic box with side length L and periodic boundary conditions. This leads to quantized momenta $\frac{2\pi}{L}\vec{n}$, $\vec{n} \in \mathbb{Z}^3$. As a consequence, the loop integrations of the infinite volume case are replaced by sums. If loop sums are divergent, they are regulated by a cutoff Λ similar to the infinite volume case.

While the finite volume modifies the infrared regime of the theory by introducing the low-momentum scale $2\pi/L$, the ultraviolet behavior does not change. Therefore, its renormalization is the same in the finite and infinite volume cases. Of course, this statement is only valid as long as the infrared and ultraviolet regime of the theory characterized by the scales $2\pi/L$ and Λ , respectively, are well separated, i.e., $\Lambda L \gg 1$. We will explicitly demonstrate that the numerical results in this publication are indeed renormalized. The cutoff dependence in the two-body sector can be removed completely by matching the coupling constant g_2 to a low-energy two-body observable, namely the two-body scattering length a or, if applicable, the two-body binding energy. As the cutoff is increased, the three-body coupling approaches a renormalization group limit cycle, leading to a log-periodic dependence of the coupling constant g_3 on the cutoff Λ . For convenience, g_3 is often expressed in terms of a dimensionless function H via $g_3 = -9g_2^2 H(\Lambda)/\Lambda^2$. The phase of the log-periodic dependence of H has to be fixed from a three-body datum [16–18, 28].

The central quantity in the three-body sector is the boson-diboson amplitude. The derivation of the equation governing this object in finite volume has been shown in detail in a previous publication [20, 22] and is therefore only briefly sketched in the following. A discussion of the infinite-volume case can be found, e.g., in [17, 28]. Starting point for both cases is the Lippmann-Schwinger equation for the boson-diboson amplitude. In a finite volume, there is no continuous scattering spectrum, but only discrete energy levels. The analytic structure of the amplitude is given by a number of simple poles at the energies of these discrete states, just like the analytic structure of bound states in the infinite volume. In addition, the incoming and outgoing quantum numbers separate. The residue at the pole is the amplitude \mathcal{F} . Comparing the residues of both sides of the Lippmann-Schwinger equation at any

of the discrete energy levels yields the homogeneous equation depicted diagrammatically in Figure 1.

In the center of mass frame, the momenta of the outgoing single boson and diboson are \vec{p} and $-\vec{p}$, respectively. The outgoing single boson is taken to be on-shell, giving the four-momentum $(p^2/2, \vec{p})$. The four-momentum of the outgoing diboson line is $(E - p^2/2, -\vec{p})$, making the total kinetic energy E a parameter of the equation. The equation depicted in Fig. 1 then serves as a consistency condition. Values of the energy parameter E for which the equation has a solution are identified as the energies of the discrete finite volume spectrum.

Using the kinematics outlined above, the sum equation for the boson-diboson amplitude \mathcal{F} reads

$$\mathcal{F}(\vec{p}) = \frac{8\pi}{L^3} \sum_{\vec{q} \in \frac{2\pi}{L}\mathbb{Z}^3}^{\Lambda} \mathcal{Z}(E; \vec{p}, \vec{q}) \tau(E; q) \mathcal{F}(\vec{q}). \quad (2)$$

The quantity $\mathcal{Z}(E; \vec{p}, \vec{q})$ contains the interaction kernel of the sum equation, while $\tau(E; q)$ is essentially the diboson propagator inside the loop.

For the diboson lines in the three-body equation depicted in Fig. 1, the interacting diboson propagator has to be used. This quantity is obtained by dressing the bare propagator, which is a constant, with bosonic loops (cf. [18]). In the sum equation (2), it appears via the quantity [19, 22]

$$\tau(E; q) = \left(\frac{1}{a} - \sqrt{\frac{3q^2}{4} - E} + \sum_{\substack{\vec{j} \in \mathbb{Z}^3 \\ \vec{j} \neq \vec{0}}} \frac{1}{L|\vec{j}|} e^{-|\vec{j}|L\sqrt{\frac{3q^2}{4} - E}} \right)^{-1}, \quad (3)$$

which is identical to the full propagator up to a prefactor. The absolute value of the integer three-vector \vec{j} is denoted $|\vec{j}|$. In the limit $L \rightarrow \infty$, the propagator reduces to the infinite volume expression.

The interaction kernel is given by the one-boson exchange term and the boson-diboson contact interaction. Since the time direction is considered to be of infinite extent, the integration over the loop energy remains continuous and can be performed analytically by using the residue theorem. The resulting interaction kernel depends only on incoming and outgoing three-momenta as well as the total energy:

$$\mathcal{Z}(E; \vec{p}, \vec{q}) = \left[\frac{1}{p^2 + \vec{p} \cdot \vec{q} + q^2 - E} + \frac{H(\Lambda)}{\Lambda^2} \right] \quad (4)$$

In the present calculation, only energies below the threshold for the break-up into three individual bosons, i.e. $E < 0$, are considered. This keeps the investigated states below any inelastic thresholds, in particular the $Nd \rightarrow NNN$ threshold.

B. Methodology

The amplitude \mathcal{F} is strictly speaking only defined for the discrete momenta inside the box. One ansatz for the solution of the sum equation (2) is therefore to use the quantized momenta themselves as sampling points. In this approach, the value of the amplitude at the sampling points is written as $f_i = \mathcal{F}(\vec{p}_i)$, where the index i labels all momenta $p_i \in \frac{2\pi}{L^3}\mathbb{Z}^3$

ℓ	m	$C_{A_1\ell m}$	$K_{A_1\ell}(\hat{p})$
0	0	1	1
4	0	$\frac{\sqrt{21}}{6}$	$\frac{5\sqrt{21}}{4} (\hat{p}_1^4 + \hat{p}_2^4 + \hat{p}_3^4 - \frac{3}{5})$
4	$\pm 1, 2, 3$	0	
4	± 4	$\frac{\sqrt{30}}{12}$	

TABLE I. Coefficients $C_{A_1\ell m}$ of the cubic harmonics [31] as well as $K_{A_1\ell}$ in Cartesian coordinates [29] for $\ell = 0, 4$.

with $|\vec{p}_i| < \Lambda$. This yields the finite-dimensional eigenvalue equation

$$f_i = \sum_j \left[\frac{8\pi}{L^3} \mathcal{Z}(E; \vec{p}_i, \vec{q}_j) \tau(E; |\vec{q}_j|) \right] f_j \quad (5)$$

The range of box side lengths that allow for the use of this ansatz is limited. The number of points to consider roughly scales as $(\Lambda L)^3$, while the complexity of the necessary matrix diagonalization scales like the number of points to the third power. We will therefore only show results for $L \leq a$ in this publication. Another drawback of this approach is that it is cumbersome to disentangle the contribution of different partial waves to the finite volume spectrum. We will refer to this ansatz as the *Grid approach*.

The momentum quantization inside a finite volume is tantamount to a reduction of the spherical symmetry of the infinite volume to a discrete symmetry, namely in our case the point symmetry of the cube. In the language of group theory, the infinitely many irreducible representations of the rotational group $SO(3)$ become reducible in terms of the five irreducible representations of the cubic group O . Hence, a quantity ψ_s transforming according to the irreducible representation s of O can be written in terms of the basis functions of spherical symmetry, i.e. spherical harmonics $Y_{\ell m}$, via

$$\psi_s(\vec{p}) = \sum_{\ell, t} R_{\ell t}(p) K_{s\ell t}(\hat{p}), \quad \text{with } K_{s\ell t}(\hat{p}) = \sum_m C_{s\ell m}^{(t)} Y_{\ell m}(\hat{p}), \quad (6)$$

where $\hat{p} = \vec{p}/p = (\hat{p}_1, \hat{p}_2, \hat{p}_3)$ is the unit vector in \vec{p} -direction and $R_{\ell t}$ is the radial function. The index t is needed if the representation labeled by ℓ appears in the irreducible representation s more than once. The coefficients $C_{s\ell m}^{(t)}$ are real and normalized for given values of s , ℓ and t via $\sum_m \left[C_{s\ell m}^{(t)} \right]^2 = 1$. The linear combinations $K_{s\ell t}$ of spherical harmonics are called “kubic harmonics” (sic!) [29]. The values of the coefficients $C_{s\ell m}^{(t)}$ are known for ℓ as large as 12 [30] and are readily computed from group theory [31]. In this work, we restrict ourselves to amplitudes \mathcal{F} transforming under the trivial (A_1) representation of the cubic group, because it contains the trivial representation of spherical symmetry, namely $\ell = 0$. This is because the investigated Efimov states are S-wave states in the infinite volume. In addition, A_1 receives contributions from $\ell = 4, 6, 8, \dots$. Since all ℓ -values appear only once below $\ell = 12$, the index t is dropped in the following. The coefficients $C_{A_1\ell m}$ for $\ell = 0, 4$ are summarized in Table I together with the resulting cubic harmonics in Cartesian coordinates, normalized to 4π .

The expansion of the angular dependence of the amplitude in spherical harmonics allows for an assessment of the impact of higher partial waves or, in other words, of the loss of

spherical symmetry in the finite volume. Moreover, it allows for an analytic calculation of the angular dependence, leaving only the radial part for a numerical treatment. This significantly reduces the complexity of the numerical problem at hand compared to the Grid approach. We therefore determine the \hat{p} -dependence of the right hand side of Eq. (2). The only quantity where \vec{p} is present is the one-boson exchange part of the interaction kernel $\mathcal{Z}(E; \vec{p}, \vec{q})$, given by the first term in Eq. (4). Consider therefore the quantity

$$I_p^{(\ell)}(\vec{q}) = \int_{S^2} \frac{d^2\hat{p}}{4\pi} K_{A_1\ell}(\hat{p}) \left[\sum_{C \in O} \left(\frac{1}{\alpha + \vec{p} \cdot C\vec{q}} + \frac{1}{\alpha - \vec{p} \cdot C\vec{q}} \right) \right], \quad (7)$$

where we have set $\alpha = p^2 + q^2 - E$ for simplicity. The summation of all elements of the cubic group O makes the expression in square brackets invariant under any cubic rotation of \vec{p} and \vec{q} . It therefore transforms according to the trivial representation, denoted A_1 , of the cubic group. The inclusion of the second term makes it moreover invariant under additional parity transformations. The expansion coefficients of this quantity in cubic harmonics are given by $I_p^{(\ell)}(\vec{q})$. The analytic evaluation of the angular integral is shown in Appendix A. The result is

$$I_p^{(\ell)}(\vec{q}) = \frac{48}{pq} Q_\ell \left(\frac{\alpha}{pq} \right) K_{A_1\ell}(\hat{q}), \quad (8)$$

where Q_ℓ is the ℓ th Legendre function of the second kind as defined in [32]. Special care has to be taken of the limiting cases $p, q \rightarrow 0$. The result $I_0(\vec{q}) = I_p(\vec{0}) = \frac{48}{\alpha} \delta_{\ell 0}$ coincides with the zero-momentum limit of (8).

We will now use this result to simplify – at least from a numerical viewpoint – the sum equation (2). The summation over the discrete set of three-vectors can be rewritten in terms of a summation over the elements of the cubic group as follows:

$$\sum_{\vec{q} \in \frac{2\pi}{L} \mathbb{Z}^3} f(\vec{q}) = \sum_{\vec{q} \in \frac{2\pi}{L} \langle \mathbb{Z}^3 \rangle} \frac{\text{mul}(\vec{q})}{48} \sum_{C \in O} (f(C\vec{q}) + f(-C\vec{q})), \quad (9)$$

where $\langle \mathbb{Z}^3 \rangle = \{\vec{q} \in \mathbb{Z}^3 : q_1 \geq q_2 \geq q_3 \geq 0\}$. All other vectors in \mathbb{Z}^3 can be generated by applying cubic rotations and the parity operator to the vectors in $\langle \mathbb{Z}^3 \rangle$, i.e.,

$$\bigcup_{C \in O} (C + CP) \langle \mathbb{Z}^3 \rangle = \mathbb{Z}^3. \quad (10)$$

However, the summation over all cubic rotations in (9) might introduce double counting. Specifically, if the original vector contains identical entries or zeroes, several cubic rotations have the same image vector. This is accounted for by the factor $\text{mul}(\vec{q})/48$, where $\text{mul}(\vec{q})$ is the number of vectors that contain the same entries as \vec{q} up to ordering and signs. The identity Eq. (9) was also used to reduce the dimensionality in the numerical implementation

of the Grid approach. Applying (9) to Eq. (2) yields

$$\begin{aligned}
\mathcal{F}(\vec{p}) &= \sum_{\ell}^{(A_1)} R_{\ell}(p) K_{A_1 \ell}(\hat{p}) = \frac{8\pi}{L^3} \sum_{\vec{q} \in \frac{2\pi}{L} \langle \mathbb{Z}^3 \rangle} \frac{\text{mul}(\vec{q})}{48} \tau(E; q) \mathcal{F}(\vec{q}) \sum_{C \in O} (\mathcal{Z}(E; \vec{p}, C\vec{q}) + \mathcal{Z}(E; \vec{p}, -C\vec{q})) \\
&= \frac{8\pi}{L^3} \sum_{\vec{q} \in \frac{2\pi}{L} \langle \mathbb{Z}^3 \rangle} \left(\frac{1}{pq} \sum_{\ell}^{(A_1)} Q_{\ell} \left(\frac{p^2 + q^2 - E}{pq} \right) K_{A_1 \ell}(\hat{p}) K_{A_1 \ell}(\hat{q}) + \frac{H(\Lambda)}{\Lambda^2} K_{A_{10}}(\hat{p}) \right) \\
&\quad \times \text{mul}(\vec{q}) \tau(E; q) \mathcal{F}(\vec{q}),
\end{aligned} \tag{11}$$

where the ℓ -sums run over the partial waves contained in the A_1 -representation, denoted by the upper summation limit (A_1) , and $\mathcal{F}(C\vec{q}) = \mathcal{F}(\vec{q}) \forall C \in O$ was used in the first line.

Comparing the coefficients of $K_{A_1 \ell}(\hat{p})$ in Eq. (11) yields a set of coupled equations for the radial functions R_{ℓ} . Let $R_{\ell i} = R_{\ell}(p_i)$, where the p_i are the possible absolute values of vectors in $\frac{2\pi}{L} \mathbb{Z}^3$ smaller than the cutoff Λ . The resulting expression has the form of an eigenvalue problem

$$R_{\ell i} = M_{\ell i; \ell' j}(L; E) R_{\ell' j}, \tag{12}$$

where the matrix M is given by

$$\begin{aligned}
M_{\ell i; \ell' j}(L; E) &= \frac{8\pi}{L^3} \sum_{\substack{\vec{q} \in \frac{2\pi}{L} \langle \mathbb{Z}^3 \rangle \\ |\vec{q}|=q_j}}^{\Lambda} \left[\frac{1}{p_i q_j} Q_{\ell} \left(\frac{p_i^2 + q_j^2 - E}{p_i q_j} \right) K_{A_1 \ell}(\hat{q}) + \frac{H(\Lambda)}{\Lambda^2} \delta_{\ell 0} \right] \\
&\quad \times \text{mul}(\vec{q}) \tau(E; q_j) K_{A_1 \ell'}(\hat{q}).
\end{aligned} \tag{13}$$

We use a root finding algorithm to determine values of the energy parameter E such that the eigensystem (12) contains an eigenvalue 1, yielding the discrete energy levels inside the finite volume.

For the discussion of the perturbative approaches, it will be convenient to write the matrix equation (12) in block matrix form in angular momentum space, viz.

$$\begin{pmatrix} R_0 \\ R_4 \\ \vdots \end{pmatrix} = \begin{pmatrix} M_{00} & M_{04} & \dots \\ M_{40} & M_{44} & \dots \\ \vdots & \vdots & \ddots \end{pmatrix} \begin{pmatrix} R_0 \\ R_4 \\ \vdots \end{pmatrix}, \tag{14}$$

with $(R_{\ell})_i = R_{\ell i}$ and $(M_{\ell \ell'})_{ij} = M_{\ell i; \ell' j}$. The dependence of the block matrices on the box side length and the energy parameter is suppressed in this notation. The off-diagonal block matrices in (14) are responsible for the mixing of different partial waves.

We will refer to the method described above as the *Sum approach*. The conceptual advantage of this approach is the possibility to disentangle the contributions of the different partial waves to the energy shift in the finite volume. On the numerical side, the dimensionality of the eigenvalue problem is greatly reduced in comparison to the Grid approach: if there are several three-momenta with identical absolute value, they all increase the dimensionality of the Sum approach only by one. The differences in dimensionality and runtime will be discussed at the end of Section III.

In earlier works [19, 20, 22] the loop sum was rewritten into a sum of integrals via the Poisson equation. This explicitly recovers the infinite volume form of the amplitude. This is appropriate for bound states, where this approach was used. It is, however, not appropriate when extending the formalism into the energy region of elastic boson-diboson scattering. Here, the infinite and finite volume amplitudes have fundamentally different analytic structures, namely a scattering continuum and a series of poles corresponding to a discrete spectrum, respectively. This energy region is accessible with the new Sum approach. We will refer to the older approach as the *Poisson approach*.

C. Perturbative approaches

In the infinite volume, bound states and low-lying scattering states are predominantly S-wave states. In the finite volume, there are admixtures from higher partial waves stemming from the breakdown of the spherical symmetry, as discussed above. For reasonably large volumes, these admixtures are expected to be small compared to the S-wave only part.

To see that this is indeed the case, consider the argument of the Legendre function Q_ℓ in the definition of the matrix elements (13). The argument $(p_i^2 + q_j^2 - E)/(p_i q_j)$ is guaranteed to be larger than 1 (remember that $E < 0$ here) and will be large if the ratio p_i/q_j is either very large or very small. For large arguments $z \gg 1$, the Legendre functions $Q_\ell(z)$ scale as $z^{-\ell-1}$ (see, e.g., [32]). Therefore,

$$\frac{Q_4(z)}{Q_0(z)} \sim z^{-4}, \text{ if } z \gg 1, \quad (15)$$

which shows the suppression of the G-wave contributions. The momenta p_i, q_j are multiples of the low-momentum scale $2\pi/L$. Consider, for example, the pair of momenta with the largest possible ratio, namely Λ and $\frac{2\pi}{L}$. With these choices, and the condition $\Lambda L \gg 1$ from renormalizability, the argument of the Legendre function becomes $\frac{L}{2\pi}(\Lambda + (E_3/\Lambda))$. Using the expansion of the Legendre functions for large arguments, we can estimate the scaling of the G-wave correction by

$$\frac{Q_4}{Q_0} \sim \left(\frac{2\pi}{\Lambda L}\right)^4. \quad (16)$$

The scaling of other matrix elements with the box side length is not as drastic but still governed by the strong suppression evidenced in Eq. (15).

A second suppression mechanism comes from the cubic harmonics in the definition of the matrix elements (13). While the cubic harmonic K_{A_10} is just a constant, the corresponding functions for $\ell \neq 0$ show sign oscillations (cf. Table I). These lead to cancellations among the terms from vectors with the same absolute value. These corrections are themselves independent of the size of the volume as they reflect the breakdown of the spherical symmetry. However, there are more cancellations among integer vectors of high absolute values, where the number of vectors with identical absolute value is large. These vectors are reached for $\Lambda L \gg 1$, leading to more cancellations within the summation over the possible momenta.

Overall, the two suppression mechanisms in the definition of the matrix elements introduce the generic hierarchy

$$M_{00} \gg M_{04} \gg M_{40} \gg M_{44} \gg M_{60} \gg \dots \quad (17)$$

In the following, we discuss two different approaches to take advantage of this ordering. The first one can be described as a partially resummed calculation, while the second approach is developed as a strict perturbative expansion. In the following discussion, we will use the notation introduced in Eq. (14).

For the *Partial Resummation approach*, consider the second row of Eq. (14),

$$R_4 = M_{40}R_0 + M_{44}R_4 + \dots \quad (18)$$

Inserting this expression for R_4 into the equation for R_0 given by the first row of Eq. (14) yields the term $M_{04}M_{44}R_4$ containing an additional factor of $K_{A_14}(\vec{q})$ compared to $M_{04}M_{40}R_0$. This term is therefore discarded as parametrically small in the partial resummation approach. More generally, the partial wave amplitudes R_ℓ for $\ell \neq 0$ are approximated by $R_{\ell \neq 0} = M_{\ell 0}R_0$, or equivalently by setting all $M_{\ell \neq 0, \ell' \neq 0}$ to zero:

$$\begin{pmatrix} R_0 \\ R_4 \\ \vdots \end{pmatrix} \simeq \begin{pmatrix} M_{00} & M_{04} & \dots \\ M_{40} & 0 & 0 \\ \vdots & 0 & 0 \end{pmatrix} \begin{pmatrix} R_0 \\ R_4 \\ \vdots \end{pmatrix} \implies R_0 \simeq \left(M_{00} + \sum_{\ell \neq 0} M_{0\ell}M_{\ell 0} \right) R_0, \quad (19)$$

where the sum over ℓ is truncated at $\ell = 0$ or $\ell = 4$ in the calculations presented in this paper. This is possible due to the general hierarchy (17). Using this equation, the energy of the state can be obtained by the eigenvalue method described above.

For the *Strictly Perturbative approach*, we first establish how to obtain the perturbed energies in the eigenvalue method. Consider the general eigenvalue equation

$$T(E) = K(E) T(E) \quad (20)$$

for an amplitude T and a matrix K , where both quantities depend on a parameter E that is tuned such that T is an eigenvector of K with eigenvalue 1. If the matrix K contains a small perturbation $K(E) = K_0(E) + \varepsilon K_1(E)$ with $\varepsilon \ll 1$, both $T(E)$ and E can be expanded in powers of ε , retaining only the linear term:

$$\begin{aligned} T(E) &= T_0(E) + \varepsilon T_1(E) + \mathcal{O}(\varepsilon^2), \\ E &= E_0 + \varepsilon E_1 + \mathcal{O}(\varepsilon^2), \end{aligned} \quad (21)$$

such that

$$T_0(E_0) = K_0(E_0) T_0(E_0) \quad (22)$$

holds. Furthermore, the E -dependence of K_0 and T_0 can be linearized around E_0 as

$$\begin{aligned} K_0(E) &= K_0(E_0) + \varepsilon E_1 K_0'(E_0) + \mathcal{O}(\varepsilon^2) \\ T_0(E) &= T_0(E_0) + \varepsilon E_1 T_0'(E_0) + \mathcal{O}(\varepsilon^2), \end{aligned} \quad (23)$$

where the prime indicates differentiation with respect to the energy parameter. Inserting the expansions (21) and (23) into (20) and comparing orders of ε yields to order ε^0 just Eq. (22). To order ε^1 , we obtain

$$E_1 T_0' + T_1 = E_1 K_0' T_0 + K_1 T_0 + K_0 [E_1 T_0' + T_1], \quad (24)$$

where all quantities are evaluated at the leading order energy E_0 . Multiplying by $T_0^\dagger(E_0)$ from the left hand side and using the daggered version of Eq. (22) yields the desired equation for the energy shift in lowest order in ε

$$E_1 = -\frac{T_0^\dagger K_1 T_0}{T_0^\dagger K'_0 T_0}. \quad (25)$$

Note that the leading order amplitude T_0 appears only at the leading order energy.

In the present framework, the leading order matrix K_0 is given by the block matrix M_{00} in Eq. (14), while the leading order amplitude is accordingly the amplitude R_0 determined such that

$$R_0(E_0) = M_{00}(E_0)R_0(E_0) \quad (26)$$

holds, cf. Eq. (22). Since the dependence of M_{00} on the energy parameter is known from Eq. (13), the differentiation in the denominator of (25) can be carried out analytically. As can be read off from Eq. (19) in the discussion of the partial resummation approach, the perturbation is given by

$$K_1 = \sum_{\ell \neq 0} M_{0\ell} M_{\ell 0}, \quad (27)$$

where the sum over ℓ will again be truncated at $\ell = 4$ in our calculations.

In earlier publications [19, 20, 22], we showed how the computational effort can be reduced by expanding the matrix $M_{00}(E)$ around the infinite volume energy. Results from these calculations agree with those obtained using the full energy dependent matrix as long as the shift from the infinite volume energy is smaller than 20%. However, since these shifts are in general much larger for volume sizes typical for present day lattice calculations, this earlier approach is not applicable in the present work and therefore not followed further.

III. RESULTS AND DISCUSSION

Using the formalism laid out in the previous section, we now present the negative energy spectrum in finite cubic volumes of varying side lengths. We provide a detailed discussion of the results with emphasis on the applicability of the perturbative approaches. For convenience, the dependence of the energies on the boson mass m is reinstated in the following.

In this publication, we focus on systems with a positive two-body scattering length a . In such systems, a physical diboson state with the energy $E_D = -1/(ma^2)$ exists in the infinite volume. This energy constitutes the threshold for the break-up of a triboson into a diboson and a single boson. The volume dependence of the diboson in a finite cubic box is derived in [10, 33]. The threshold for the break-up into three single bosons is given by $E = 0$.

We investigate four states with different energies in the infinite volume:

- **State A:** $E_3^\infty = -10/(ma^2)$
- **State B:** $E_3^\infty = -5/(ma^2)$
- **State C:** $E_3^\infty = -3/(ma^2)$
- **State D:** $E_3^\infty = -1.5/(ma^2)$

In these “universal units”, the energy of the three-body state is given in units of the two-body bound state, which is physical for $a > 0$ and virtual for $a < 0$.

For each of these states, the finite volume spectrum has been calculated for several values of the box side length L . In applications of the formalism to Lattice QCD, the volume under consideration will be smaller than the unnaturally large scattering length. Therefore, we concentrate on the region $L \leq a$ and show results for various box side lengths between $L = a$ and $L = 0.25a$.

In order to provide an understanding of the universal units employed in this publication, we take a look at the nucleonic sector. There, two spin-isospin channels with associated scattering lengths $a_{1S_0} = -23.7$ fm and $a_{3S_1} = 5.4$ fm are present. Using a “middle ground” of 15 fm for the unnaturally large scattering length, we see that the investigated volume range contains typical volume sizes of present day Lattice QCD calculations, which are about 2.5 fm to 4 fm. The triton energy in units of the deuteron binding energy is $E_T = -3.8E_D$, placing this state roughly between the states B and C. Note, however, that all results presented in this paper are for bosonic systems.

In order to explicitly verify that our results are renormalized, we use different cutoffs Λ . For all cutoffs considered, the three-body force parameterized by $H(\Lambda)$ has been fixed such that the same infinite volume energy is obtained. If our results are indeed renormalized, the results for the different cutoffs should agree with each other up to an uncertainty of the order $1/(\Lambda a)$ stemming from the finiteness of the cutoff. In lattice simulations, the scale for the cutoff is set by the edge of the first Brillouin zone given by π/b , where b is the lattice spacing. The cutoffs employed in this calculation, $\Lambda a = 314$ and $\Lambda a = 225$, correspond to typical present day lattice spacings of $b = 0.1$ fm and $b = 0.15$ fm, respectively.

We investigated five different variants. The Grid approach from Eq. (5) is the exact result. All other runs employ the Sum approach. The leading order of our perturbative approaches is obtained by only taking S-wave contributions into account (cf. Eq. (26)). The three remaining runs include the G-wave ($\ell = 4$) using the full equation (12) as well as the two perturbative approaches (cf. Eqs. (19), (25)) described above.

The volume dependence of the investigated states is depicted in the left panels of Fig. 2 for the Grid approach as well as the S-wave and full G-wave calculation in the Sum approach. The infinite volume energy of the state is shown as a star on the left axis. The curves for different cutoffs agree with each other to within better than 1%, indicating proper renormalization of the results. There is no visible difference between the three depicted variants for all investigated volumes.

The curves show the qualitative behavior known from our previous work for box side lengths down to $L = 0.5a$ [19, 20, 22]. When decreasing the volume size from infinity, the state remains unaffected at first. Going below a certain box size starts to affect the state strongly, which is in line with the expected exponential behavior of finite volume corrections for bound states. The box size below which the state shows strong deviations from its infinite volume energy is tied to the spatial extent of the state in the infinite volume, which can be estimated as $(-mE_3^\infty)^{-1/2}$. The size of the state is also correlated with the length scale in the exponential behavior of the finite volume corrections.

To see that this is indeed the case, we summarize the finite volume shifts at $L = a$ calculated using the Grid approach for all four states and the two investigated cutoffs Table II. The results for the two cutoffs agree with each other, again showing that the finite volume results are renormalized. Comparing the shifts, we notice that state A is shifted by 45%, while the more shallow and, therefore, larger state B is already shifted by 137%. For all

State	$E_3^\infty ma^2$	$(-mE_3^\infty)^{-1/2}$	$\Lambda a = 225$ $E_3(L = a) ma^2$	$\Lambda a = 314$ $E_3(L = a) ma^2$	δ_{rel}
A	-10	0.32 a	-14.49	-14.49	44.9%
B	-5	0.45 a	-11.87	-11.87	137.4%
C	-3	0.58 a	-10.63	-10.63	254.3%
D	-1.5	0.82 a	-8.28	-8.28	452.0%

TABLE II. Comparison of infinite volume energies and finite volume energies at $L = a$ as calculated by the Grid approach. Shown are results for the two different cutoffs along with the relative deviation from the infinite volume energy $\delta_{\text{rel}} = (E_3(L = a)/E_3^\infty) - 1$. Also shown is the size estimate $(-mE_3^\infty)^{-1/2}$.

states except the deepest state A the relative deviation from the infinite volume energy exceeds 100%. It is even larger than 400% for the shallowest state D. The shift at $L = a$ is strongly dependent on the size of the state in the infinite volume, and therefore on the infinite volume energy. Thus, a given finite volume affects a shallow state with a large spatial extent more than smaller, more deeply bound state, as expected.

The volume dependence of the three-body energy as shown in the left panels of Fig. 2 seems identical for the three plotted approaches. However, there are small differences between the different runs. We use the exact result from the Grid approach as a baseline and also present the differences $\Delta E_3(L) = E_3^{(\text{Sum})}(L) - E_3^{(\text{Grid})}(L)$ in the right panels of Fig. 2. Here, $E_3^{(\text{Sum})}$ can be any of the four runs employing the Sum approach. Namely, these are the S-wave only calculation, the full calculation including the G-wave and the two perturbative approaches.

The differences to the respective baseline appear cutoff independent. Some variation is visible in the Strictly Perturbative treatment, but it is within the uncertainty from the finiteness of the cutoff which is of the order $1/(\Lambda a)$.

The full results with and without the G-wave as well as the partially resummed results are always larger than the Grid results. The S-wave only result in general deviates from the Grid result by more than $0.001/(ma^2)$. The inclusion of the G-wave consistently reduces the difference to the full Grid result by about two orders of magnitude. In other words, the inclusion of higher partial waves lowers the energy of the investigated state.

For the very deeply bound state A, the difference between the respective Sum approach runs and the Grid approach does only weakly depend on the volume. For volumes with side lengths larger than $L = a/2$, state B shows the same qualitative behavior. Below $L = a/3$, the difference between the Sum approach and the Grid approach becomes larger, but is still very small compared to the energy of the state itself. This can be understood as higher partial waves with $\ell \geq 6$ having a larger and larger contribution. In addition, the absolute size of the G-wave contribution strongly increases, as expected, when going to smaller volumes.

Turning to state C, we observe a behavior similar to that of state B. The strong increase in the spread between the Sum approach runs and the Grid approach as well as in the size of the G-wave contribution starts at a larger volume, namely around $L = 0.6a$. This reflects the larger spatial extent of the more shallowly bound state C compared to state B. The differences of the Sum approach to the Grid results grow by two orders of magnitude within the investigated volume range. For the full result, for example, the difference increases from

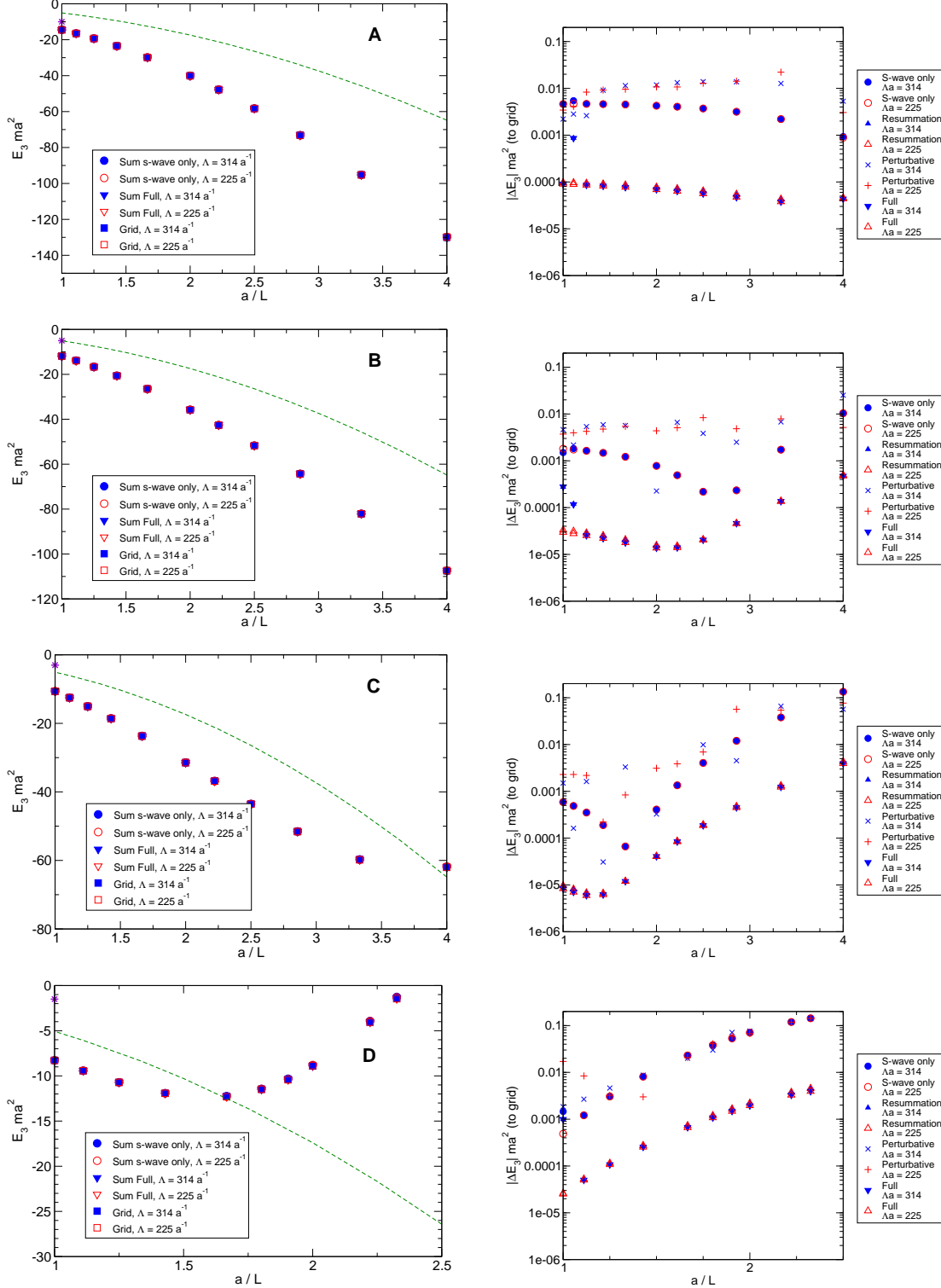


FIG. 2. *Left:* Variation of the three-body energy E_3 with the box side length L for two cutoffs. Plotted are the Sum approach with S-wave only and including the G-wave as well as the Grid approach. The infinite volume energy is marked as a star on the left axis. The dashed line is the two-body energy. *Right:* Difference between the Grid approach and the Sum approach results (S-wave only and including the G-wave via full calculation, partial resummation and strict perturbation theory). Note the different volume range in the last row.

$10^{-5}/(ma^2)$ at $L = a$ to $0.004/(ma^2)$ at $L = a/4$. For the very shallow state D, we observe a strong increase of the differences when going towards smaller volumes. They also grow by two orders of magnitude, albeit over a much smaller volume range. The difference of the full result at $L = a$ is $2 \times 10^{-5}/(ma^2)$, about twice as large as for state C. It has grown by two orders of magnitude to $0.004/(ma^2)$ already at $L = 0.43a$.

The size of the higher partial wave contributions is comparable to the uncertainty due to the finiteness of the cutoff, which is of order $1/(\Lambda a)$. This should change when including higher orders of the EFT. The next-to-leading order corrections are governed by the effective range r_e and are of the order r_e/a and kr_e , where k is a typical momentum. Their inclusion will be part of the extension of this framework to the three-nucleon system.

Overall, the G-wave and higher corrections are indeed small compared to the S-wave energies, justifying their perturbative treatment. In particular, the partial resummation approach captures the G-wave corrections almost completely. More than 99% of the shift from the S-wave result to the full result are accounted for using this approach.

For sufficiently large box sizes, states C and D show a different volume dependence than the more deeply bound states (bottom left panels of Fig. 2). For both states, we find energies above the two-body energy depicted by the dashed line. For state C, this is the case for the smallest investigated volume $L = a/4$ only. The data points for $L = 0.3a$ suggest a flattening out of the volume dependence, allowing the two-body energy to catch up when further decreasing the box size. This is more clearly seen in the volume dependence of state D. At $L = 0.6a$, the two- and three-body energy in the finite volume are equal. For smaller volumes, the three-body state is found above the two-body state. Decreasing the volume further increases the energy of the state, until it reaches the three-body breakup threshold $E = 0$ for a volume with side length $L = 0.43a$. We also observed this behavior in the framework developed earlier [20, 22].

Our interpretation is that, as the two-body energy reaches the three-body energy, the state behaves like a boson-diboson scattering state when further shrinking the volume. Indeed, the data points above the threshold are compatible with a power-law behavior that is known to describe two-body scattering. Note, however, that we are not in the Lüscher limit $L \gg a$ and therefore do not expect a leading $1/L^3$ behavior [10]. The presence of three-body effects in the volume dependence of such a state will be the subject of further study. It was recently shown that, in this case, a topological phase is to be expected [34].

The volume size at which this crossing happens is again tied to the infinite volume energy. State D has a smaller infinite volume binding energy, and therefore a larger spatial extent. Thus, the box which is not able to hold the complete three-body bound state is larger than for the smaller state C.

Turning back to the differences shown in the right panels of Fig. 2, we note that the volume dependence of the higher partial wave contributions does not show any distinctive features at the crossover box sizes.

In the following, we compare the Poisson approach from Refs. [20–22] to the approaches developed in the present paper. The values for the Poisson and Sum approach in Fig. 3 have been obtained by truncating the partial wave expansion of the angular dependence at $\ell = 0$. We observe a visible spread between the Sum approach and the Grid approach on the one hand and the Poisson approach on the other. In the Poisson approach, the sum equation (2)

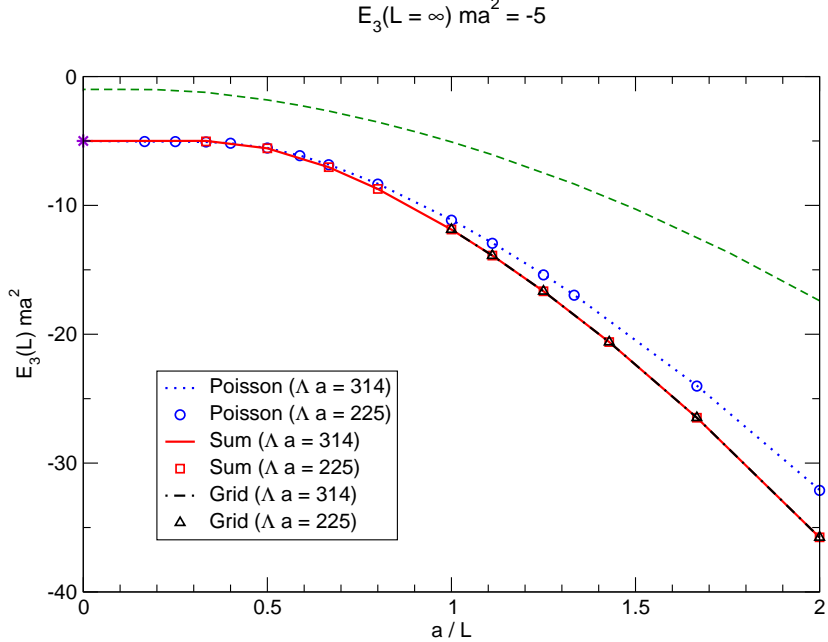


FIG. 3. Volume dependence of state B for two cutoffs, $\Lambda a = 314$ (lines) and $\Lambda a = 225$ (symbols). Shown are the exact result from the Grid approach as well as the S-wave only results from the Sum approach and the Poisson approach. The infinite volume energy $E_3^\infty ma^2 = -5$ is marked as a star on the left axis. The dashed line is the two-body energy.

is rewritten as

$$\begin{aligned}
 \mathcal{F}(\vec{p}) &= \frac{8\pi}{L^3} \sum_{\vec{q} \in \frac{2\pi}{L}\mathbb{Z}^3}^{\Lambda} \mathcal{Z}(E; \vec{p}, \vec{q}) \tau(E; q) \mathcal{F}(\vec{q}) \\
 &\stackrel{\text{(Poisson)}}{=} \frac{1}{\pi^2} \sum_{\vec{n} \in \mathbb{Z}^3} \int_0^\Lambda dq \left[\int d^2\hat{q} e^{iL\vec{n}\cdot\vec{q}} \mathcal{Z}(E; \vec{p}, \vec{q}) \right] \tau(E; q) \mathcal{F}(\vec{q}).
 \end{aligned} \tag{28}$$

The additional angular dependence introduced by the Fourier transformation leads to a recoupling of the partial waves in this approach. We note again that the S-wave component of the Sum approach almost completely captures the full result, as discussed before. In the Poisson approach, in contrast, the higher partial wave contributions are sizable.

This is encouraging in view of the extension of this framework to the three-nucleon system, which will be the subject of a future publication. In the old framework, we compared the volume dependence of the triton [21, 22] to results of a Lattice Chiral EFT calculation [24]. The decline of the energy observed in the latter was much stronger. The results described above indicate that this discrepancy will be at least diminished when extending the present framework to the three-nucleon system.

We close this section with a discussion of the numerical scaling of the presented approaches. The most costly operation in this framework is finding eigenvalues, which is equivalent to performing a matrix diagonalization. This is in general an $\mathcal{O}(N^3)$ process for real non-symmetric matrices of dimension $N \times N$. In both the Grid and the Sum approach, the dimensionality of the matrix is dependent on the box side length as it determines the size of the discretized momentum space. The left panel of Fig. 4 shows the number of vectors

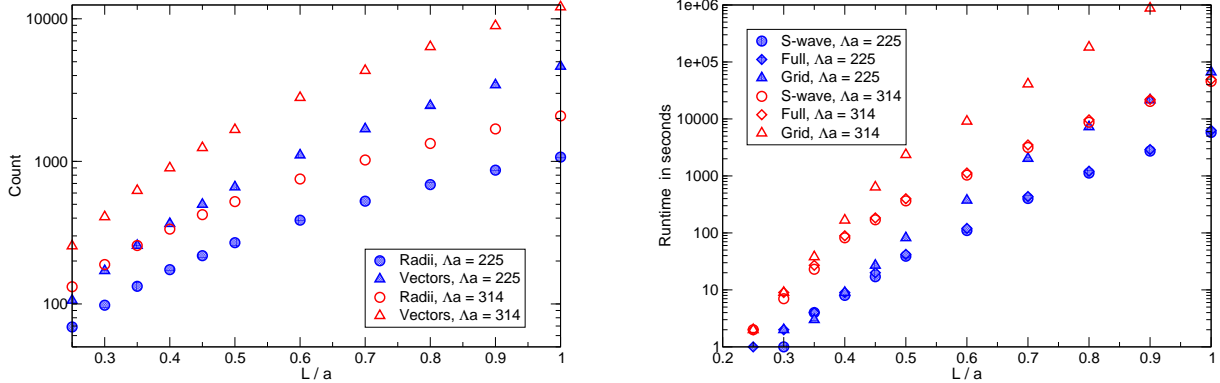


FIG. 4. Left: Number of vectors $\vec{q} \in \frac{2\pi}{L}\langle\mathbb{Z}^3\rangle$ with $|\vec{q}| < \Lambda$ and number of distinct absolute values for the two investigated cutoffs. Right: Length dependence of the runtime for three runs and two cutoffs.

$\vec{q} \in \frac{2\pi}{L}\langle\mathbb{Z}^3\rangle$ with $|\vec{q}| < \Lambda$, relevant for the Grid approach, as well as the number of distinct absolute values of these vectors, relevant for the Sum approach, for the two investigated cutoffs $\Lambda a = 225$ and $\Lambda a = 314$. As L increases, the vectors in the discrete space $\frac{2\pi}{L}\langle\mathbb{Z}^3\rangle$ lie closer to each other, eventually resembling the continuum. We therefore expect the total number of points to be proportional to the volume of a sphere, scaling as $(\Lambda L)^3$. This is indeed the case for $L > a/2$. For smaller volumes, the behavior is slightly different because the discretized space is still too “coarse”. The number of distinct radii can also be fitted to a power law, scaling like $(\Lambda L)^2$.

All results presented in this publication were obtained using a sequential implementation. The runtimes range from seconds for the smallest volumes to days for the larger volumes in the grid approach. The length dependence of the runtime is depicted in the right panel of Fig. 4 for the two cutoffs and three different runs, namely the Grid approach as well as the S-wave only and the full run in the Sum approach. The runtime of the Strictly Perturbative approach is almost identical to that of the S-wave run, while the runtime of Partial Resummation approach is comparable to that of the Sum approach including the G-wave. The scaling of the Sum approach is much better than that of the Grid approach, as expected. In the latter, the dimensionality of the matrix that has to be diagonalized in an $O(N^3)$ operation scales like $(\Lambda L)^3$ compared to $(\Lambda L)^2$ for the Sum approach. Therefore, we expect the runtime of the Grid approach to scale with three additional powers of ΛL . Indeed, fitting power laws to the runtime behavior yields a scaling of $O((\Lambda L)^7)$ for the Sum approach and $O((\Lambda L)^{10})$ for the Grid approach. The inclusion of the G-wave does not change the scaling of the code but merely increases the runtime by about 10%, independent of the cutoff. This is a significant improvement in comparison to the Poisson approach employed in previous publications, where the inclusion of the G-wave increased the runtime by a factor of 4 [20, 22]. By using parallelized code, one should be able to significantly reduce the runtime for larger volumes where the matrix dimensionality exceeds about 2000. The volume range where this is the case depends on the approach employed as well as the cutoff chosen.

IV. SUMMARY AND OUTLOOK

We studied the volume dependence of three-boson states below the three-body break-up threshold inside a cubic box with periodic boundary conditions. A new framework has been developed that provides access to the region above the boson-diboson break-up threshold and allows for a significantly faster numerical implementation of the higher partial waves. We derived an infinite set of coupled equations for the partial waves of the boson-diboson amplitude. These equations were solved for several cubic volumes with side lengths ranging from $L = a$ to $L = a/4$. Proper renormalization of the results was explicitly verified. We studied the effects from higher partial waves and found them to be comparable to the variation due to the use of a finite cutoff. We showed how these contributions can be treated perturbatively, either by partial resummation or by the use of perturbation theory for the eigenvalue equation. Both approaches yield results that are in good agreement with the full calculation, with the former performing slightly better and the latter offering a significant reduction of runtime. This is an improvement compared to our previous framework where higher partial waves play a more pronounced role and their numerical treatment is more tedious.

The next step is to extend the framework to the three-nucleon system and include higher orders of the EFT. The latter is necessary in order to perform precision extrapolations of finite volume results. Work in this direction is in progress and will be the subject of a future publication. With the new framework, it is also possible to study states that extrapolate to a scattering state in the infinite volume. This also allows one to examine, for example, three-body effects in Lattice QCD simulations of nucleon-deuteron scattering. In related work, it was shown that the compositeness of the deuteron yields modifications of topological nature to Lüscher's formula [34].

We note that an extension of the Lüscher formula relating the infinite volume scattering phase shifts to the discrete energy levels in a finite volume [10] is implicitly contained in our work. It provides the framework to determine the low-energy constants of pionless EFT in the two- and three-body sector from discrete energy levels in a cubic box. After this has been done, the infinite-volume scattering observables can be calculated in pionless EFT.

In summary, our results demonstrate that the finite volume corrections for systems of three identical bosons are calculable and under control. The role of higher partial waves was assessed and their effect was shown to be of highly perturbative nature. With high statistics Lattice QCD simulations of three-baryon systems within reach [2, 12], the calculation of the structure and reactions of light nuclei appears feasible in the intermediate future.

ACKNOWLEDGMENTS

We thank Hans-Werner Hammer for valuable discussions and for providing computational infrastructure. A large part of the calculations has been performed on the CPU cluster at the HISKP, University of Bonn. This work was supported in part by the National Science Foundation under CAREER award PHY-0645498, by the US-Department of Energy under contract DE-FG02-95ER-40907, and by University Facilitating Funds of the George Washington University.

Appendix A: Derivation of Eq. (8)

The partial wave components of the one-boson exchange part of the interaction kernel $\mathcal{Z}(E; p, q)$ are given by the quantity $I_p^{(\ell)}(\vec{q})$ defined in Eq. (7),

$$I_p^{(\ell)}(\vec{q}) = \int \frac{d^2\hat{p}}{4\pi} K_{A_1\ell}(\hat{p}) \left[\sum_{C \in O} \left(\frac{1}{\alpha + \vec{p} \cdot C\vec{q}} + \frac{1}{\alpha - \vec{p} \cdot C\vec{q}} \right) \right].$$

The integration can be carried out by expanding the cubic harmonic in terms of spherical harmonics, transforming the integration variables by a rotation R defined by $qR\hat{e}_z = C\vec{q}$ and using Wigner D-matrices:

$$\begin{aligned} I_p^{(\ell)}(\vec{q}) &= \sum_{C \in O} \sum_m C_{\ell m} \int \frac{d^2\hat{p}}{4\pi} \left(\frac{Y_{\ell m}(\hat{p})}{\alpha + \vec{p} \cdot C\vec{q}} + \frac{Y_{\ell m}(\hat{p})}{\alpha - \vec{p} \cdot C\vec{q}} \right) \\ &= \sum_{C \in O} \sum_m C_{\ell m} \int \frac{d^2\hat{p}}{4\pi} \left(\frac{Y_{\ell m}(R\hat{p})}{\alpha + R\vec{p} \cdot C\vec{q}} + \frac{Y_{\ell m}(R\hat{p})}{\alpha - R\vec{p} \cdot C\vec{q}} \right) \\ &= \sum_{C \in O} \sum_m C_{\ell m} \sum_{m'} D_{m'm}^{(\ell)}(R) \int_{-1}^{+1} \int_0^{2\pi} \frac{d \cos \theta d\phi}{4\pi} \left(\frac{Y_{\ell m'}(\hat{p})}{\alpha + pq \cos \theta} + \frac{Y_{\ell m'}(\hat{p})}{\alpha - pq \cos \theta} \right) \\ &= \sum_{C \in O} \sum_m C_{\ell m} \sum_{m'} D_{m'm}^{(\ell)}(R) N_\ell \delta_{m'0} \int_{-1}^{+1} \frac{d \cos \theta}{2} \left(\frac{P_\ell(\cos \theta)}{\alpha + pq \cos \theta} + \frac{P_\ell(\cos \theta)}{\alpha - pq \cos \theta} \right) \\ &= \sum_{C \in O} \sum_m C_{\ell m} D_{0m}^{(\ell)}(R) N_\ell \int_{-1}^{+1} d \cos \theta \frac{P_\ell(\cos \theta)}{\alpha - pq \cos \theta} \\ &= \sum_{C \in O} \sum_m C_{\ell m} \frac{1}{N_\ell} Y_{\ell m}(C\hat{q}) N_\ell \frac{2}{pq} Q_\ell \left(\frac{\alpha}{pq} \right) \\ &= \frac{2}{pq} Q_\ell \left(\frac{\alpha}{pq} \right) \sum_{C \in O} K_{A_1\ell}(C\hat{q}) \\ &= \frac{48}{pq} Q_\ell \left(\frac{\alpha}{pq} \right) K_{A_1\ell}(\hat{q}). \end{aligned} \tag{A1}$$

Here, $N_\ell = \sqrt{\frac{2\ell+1}{4\pi}}$ is the normalization constant of $Y_{\ell 0}$. The Wigner D-matrix is given by $D_{0m}^{(\ell)}(\beta, \gamma, 0) = \frac{1}{N_\ell} Y_{\ell m}(\gamma, \beta)$, where β, γ are the Euler angles of the rotation under consideration, which are by the definition of R just given by $C\hat{q}$. Further, we use a well-known integral representation of the Legendre functions of the second kind Q_ℓ [35] and, in the final step, the invariance of the $K_{A_1\ell}$ under cubic rotations.

-
- [1] S. R. Beane, K. Orginos and M. J. Savage, Int. J. Mod. Phys. E **17**, 1157 (2008) [arXiv:0805.4629 [hep-lat]].
 - [2] S. R. Beane, W. Detmold, K. Orginos and M. J. Savage, Prog. Part. Nucl. Phys. **66**, 1 (2011) [arXiv:1004.2935 [hep-lat]].

- [3] S. R. Beane, P. F. Bedaque, W. C. Haxton, D. R. Phillips and M. J. Savage, In *Shifman, M. (ed.): At the frontier of particle physics, vol. 1* 133-269 [nucl-th/0008064].
- [4] P. F. Bedaque and U. van Kolck, Ann. Rev. Nucl. Part. Sci. **52**, 339 (2002) [arXiv:nucl-th/0203055].
- [5] E. Epelbaum, Prog. Part. Nucl. Phys. **57**, 654 (2006) [arXiv:nucl-th/0509032].
- [6] E. Epelbaum, H.-W. Hammer and U.-G. Meißner, Rev. Mod. Phys. **81**, 1773 (2009) [arXiv:0811.1338 [nucl-th]].
- [7] D. R. Phillips, Czech. J. Phys. **52**, B49 (2002) [nucl-th/0203040].
- [8] R. Machleidt and D. R. Entem, Phys. Rept. **503**, 1 (2011) [arXiv:1105.2919 [nucl-th]].
- [9] M. Lüscher, Commun. Math. Phys. **104**, 177 (1986).
- [10] M. Lüscher, Nucl. Phys. B **354**, 531 (1991).
- [11] M. Lüscher, Nucl. Phys. B **364**, 237 (1991).
- [12] S. R. Beane *et al.*, Phys. Rev. D **80**, 074501 (2009) [arXiv:0905.0466 [hep-lat]].
- [13] P. F. Bedaque, H.-W. Hammer and U. van Kolck, Nucl. Phys. A **676**, 357 (2000) [arXiv:nucl-th/9906032].
- [14] H. W. Griesshammer, Nucl. Phys. A **760**, 110 (2005) [nucl-th/0502039].
- [15] V. Efimov, Phy. Lett. **33B**, 563 (1970).
- [16] H. -W. Hammer and L. Platter, Ann. Rev. Nucl. Part. Sci. **60**, 207 (2010) [arXiv:1001.1981 [nucl-th]].
- [17] E. Braaten, H. -W. Hammer, Phys. Rept. **428**, 259-390 (2006) [cond-mat/0410417].
- [18] P. F. Bedaque, H. W. Hammer, U. van Kolck, Nucl. Phys. **A646**, 444-466 (1999) [nucl-th/9811046].
- [19] S. Kreuzer and H.-W. Hammer, Phys. Lett. B **673**, 260 (2009) [arXiv:0811.0159 [nucl-th]].
- [20] S. Kreuzer and H.-W. Hammer, Eur. Phys. J. A **43**, 229 (2010) [arXiv:0910.2191 [nucl-th]].
- [21] S. Kreuzer, H. -W. Hammer, Phys. Lett. **B694**, 424-429 (2011) [arXiv:1008.4499 [hep-lat]].
- [22] S. Kreuzer, Ph.D. thesis, Universität Bonn, Germany, 2010 [http://hss.ulb.uni-bonn.de/2010/2293/2293.htm].
- [23] T. Luu, PoS **LATTICE2008**, 246 (2008) [arXiv:0810.2331 [hep-lat]].
- [24] E. Epelbaum, H. Krebs, D. Lee and U.-G. Meißner, Eur. Phys. J. A **41**, 125 (2009) [arXiv:0903.1666 [nucl-th]].
- [25] B. Borasoy, H. Krebs, D. Lee and U.-G. Meißner, Nucl. Phys. A **768**, 179 (2006) [arXiv:nucl-th/0510047].
- [26] S. Tolle, H. -W. Hammer and B. C. Metsch, Comptes Rendus Physique **12**, 59 (2011) [arXiv:1008.0551 [cond-mat.quant-gas]].
- [27] J. Rotureau, I. Stetcu, B. R. Barrett and U. van Kolck, Phys. Rev. C **85**, 034003 (2012) [arXiv:1112.0267 [nucl-th]].
- [28] L. Platter, Few Body Syst. **46**, 139 (2009) [arXiv:0904.2227 [nucl-th]].
- [29] F. C. von der Lage, H. A. Bethe, Phys. Rev. **71**, 612-622 (1947).
- [30] S. L. Altmann, A. P. Cracknell, Rev. Mod. Phys. **37**, 19-32 (1965).
- [31] V. Bernard, M. Lage, U.-G. Meissner, A. Rusetsky, JHEP **0808**, 024 (2008) [arXiv:0806.4495 [hep-lat]].
- [32] Gradshteyn, I. S. and Ryzhik, I. M., *Table of Integrals, Series and Products*, Academic Press Inc., 2007 ISBN 0-12-373637-4.
- [33] S. R. Beane, P. F. Bedaque, A. Parreno, M. J. Savage, Phys. Lett. **B585**, 106-114 (2004) [hep-lat/0312004].
- [34] S. Bour, S. Koenig, D. Lee, H. -W. Hammer, U. -G. Meissner, [arXiv:1107.1272 [nucl-th]].

- [35] M. Abramowitz, I. A. Stegun, Eds., "Handbook of Mathematical Functions," Dover Publications: New York (1972).